Nonlinear compaction of an assembly of highly deformable platelike particles

J. D. Sherwood
Schlumberger Cambridge Research, High Cross, Madingley Road, Cambridge CB3 0EL, United Kingdom

H. Van Damme
Centre de Recherche sur la Matière Divisée, Centre National de la Recherche Scientifique, and Université d'Orléans, F-45071 Orléans Cedex 02, France

(Received 25 April 1994)

A two-dimensional numerical simulation of a settling and compacting stack of platelike particles is described. The plates represent clay particles, such as are found in shales formed from sediments of clay compacted over geological time scales. The aspect ratio of a clay particle is sufficiently high that the plate is flexible when the applied stresses are large. The deformation of each plate is assumed small, and is therefore governed by the biharmonic equation. A stack of plates is first formed by ballistic deposition. The stack is then compressed uniaxially, under a gravitational stress σ_{zz}, and the stress-strain relation is obtained as a function of the flexibility of the plates. The void ratio e within the stack varies approximately as $\sigma_{zz}^{-0.3}$. Experiments are reported in which a stack of 5000 flexible paper platelets is compacted. A slightly lower power law exponent, -0.2, is found experimentally.

PACS number(s): 82.70.Dd, 81.35.+k, 83.70.Fn

I. INTRODUCTION

There have been many studies of ballistic deposition, but little is known about the deposition of nonspherical particles, and even less about the deposition of deformable particles. Our interest here lies in deposits of flat, platelike clay particles: a bentonite particle might typically have thickness $h \simeq 1$ nm and lateral dimension $L \simeq 1$ μm. Clay particles are transported by rivers to the sea, where they flocculate and form a sediment on the sea bed. Subsequent compaction over geological time scales leads to the formation of mudstones and shales [1]. Similar cakes of clay particles may be formed in the laboratory by filtration [2]. The aspect ratio L/h of the particles is sufficiently large that they are not totally rigid, and electron micrographs of shales and filtercakes frequently show that particles have deformed [3]. Here we consider both numerical simulations of flexible plates stacked on a discrete two-dimensional (2D) lattice, and experiments performed upon quasi-2D packings of flexible platelets.

We assume that the deformation of the plates is sufficiently small that standard linear theory [4] applies. If each plate has flexural rigidity D (per unit length in the y direction) and undeformed center line $z = \zeta(x) = 0$ $(0 \le x \le L)$, the energy of the plate (per unit length in the y direction) is

$$F_p = \tfrac{1}{2} D \int_0^L \left(\frac{d^2\zeta}{dx^2} \right)^2 dx \ . \tag{1}$$

This leads to the governing equation for the plate surface

$$D \frac{d^4\zeta}{dx^4} - P = 0 \ , \tag{2}$$

where P is the force per unit area acting on the plate. We shall assume that the edges $x = 0, L$ of each plate are free, leading to the boundary conditions

$$\frac{d^2\zeta}{dx^2} = 0, \quad x = 0, L \ . \tag{3}$$

As explained in [5], for a plate of thickness h and width b (in the y direction), with Young's modulus E and Poisson's ratio ν, it is appropriate to take $D = Eh^3/12(1-\nu^2)$ for a deformation which is independent of y (e.g., if $b \gg L$). If $L \gg b$, the plate may be regarded as a rod of length L with a narrow rectangular cross section, and $D = Eh^3/12$.

In Sec. II we discuss a model in which the plates are represented as a series of discrete points. In Sec. III we show how bulk macroscopic properties of the stack, such as the void ratio and stress, may be evaluated. The results of numerical simulations are presented and analyzed in Sec. IV. Finally, in Sec. V we report experimental measurements of the compaction of a stack of flexible paper platelets.

II. DISCRETE LATTICE SIMULATIONS

We consider a stack of N_p plates. We assume that the jth plate can be represented as a series of S points (x_s^j, ζ_s^j) $(s = 1, \ldots, S)$, where the x_s^j lie on a lattice $x = na$ $(n = 1, \ldots, N)$. Once the left-hand edge s=1 of the plate is fixed, the other $S-1$ points are at $x_s^j = x_1^j + (s-1)a$. During all subsequent motion and deformation of the plates, the x coordinates x_s^j are fixed, whereas the z coordinates ζ_s^j are allowed to vary continuously. This fixes the geometry of any given stack of plates, but has the disadvantage that the length of a plate depends upon its orientation. However, compaction tends to align the plates with the horizontal x axis, thereby reducing

any variation in plate length. One can picture the nodes (x_s^j, ζ_s^j) as sliding up and down a series of vertical wires $x = na$. The plates are added to the top of the stack, one at a time, at a position chosen at random. Thus no attempt is made to model the arrival of flocs (rather than individual clay particles) at the surface of the stack.

We shall consider the compaction of the stack of plates under its own weight. A gravitational force $f_g = -mga$ is assumed to act vertically at each of the nodes. The boundary condition (3) is applied at the end nodes $s = 1, S$ of the plate. To be consistent, the gravitational force at the end nodes ought to be reduced to $mga/2$, leaving a plate of length $(S-1)a$ and weight $(S-1)mga$. We shall ignore this, and consider the plate to have length $L = Sa$ and weight $Mg = Smga$. We are therefore neglecting errors introduced by applying boundary condition (3) at $s = 1, S$ rather than at $s = \frac{1}{2}, S + \frac{1}{2}$; such errors become small in the limit $S \to \infty$.

Each plate must also support the plates above, by means of contact forces. These too are discretized, and are assumed to act vertically between the node of one plate and those of the plates immediately above and below. In the simulations presented here, these contact forces were replaced by soft forces. If the vertical separation of two nodes is $\Delta\zeta$, the separation between the plate surfaces is $\Delta z = \Delta\zeta - h$, and the contact force was taken to be

$$f_z = mga(\delta/\Delta z)^2 , \tag{4}$$

with $\delta = h/100$. The initial configuration of the plates was determined by ballistic deposition onto the horizontal plane $z = 0$, using a lattice of size $N = 100$. Periodic boundary conditions in the x direction identified $x = Na$ with $x = 0$.

Each node is subjected to a force f_s^j consisting of contact forces from plates above and below, and gravity. The midpoint of each plate is at $x_c^j = (x_1^j + x_S^j)/2$. The total force F^j and couple C^j acting on each particle are given by

$$F^j = \sum_{s=1}^{S} f_s^j, \quad C^j = \sum_{s=1}^{S} f_s^j (x_s^j - x_c^j) .$$

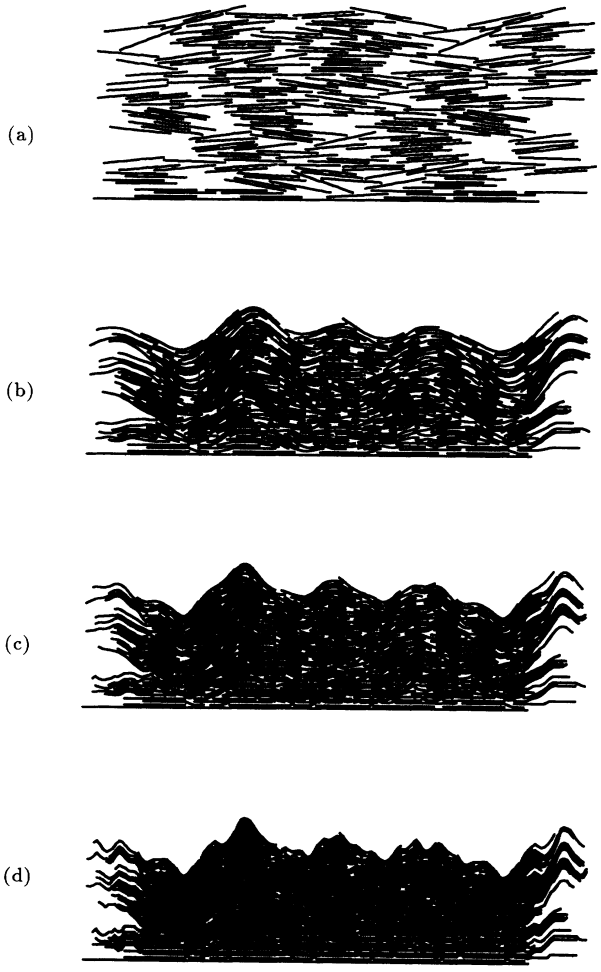

FIG. 1. Simulations of a compacted bed of 180 particles of length $L = 20a$. (a) Rigid plates; (b) $G = 1.9 \times 10^3$; (c) $G = 2.1 \times 10^4$; (d) $G = 1.8 \times 10^5$.

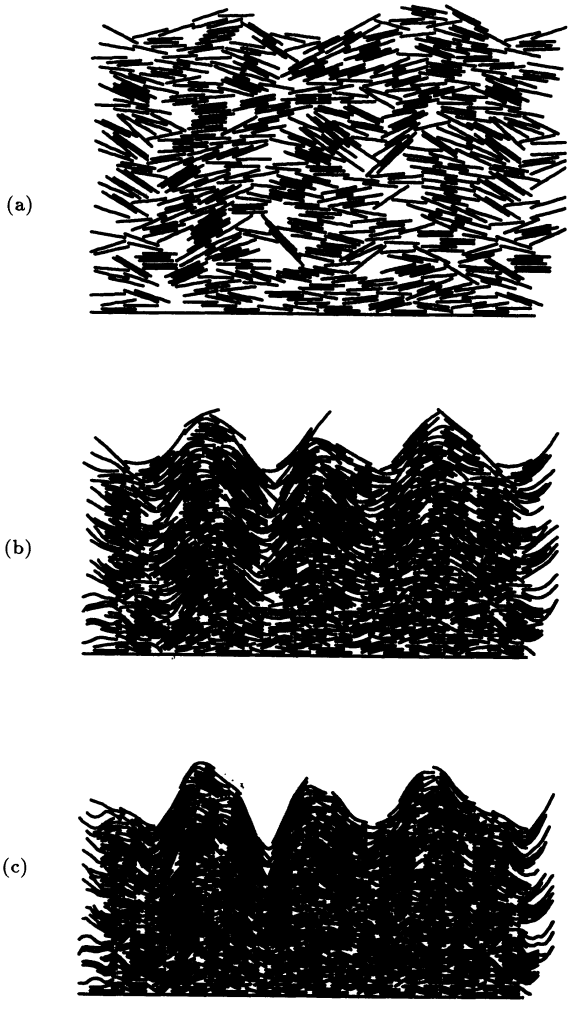

FIG. 2. Simulations of a compacted bed of 500 particles of length $L = 10a$. (a) Rigid plates: (b) $G = 1.2 \times 10^2$; (c) $G = 1.3 \times 10^3$.

The plates were allowed to sediment from their initial configuration, with translational and angular velocities proportional to F^j and C^j, respectively, until an approximate equilibrium position was found. This was then further refined by computing derivatives of F^j and C^j with respect both to vertical displacements and to rotation, and then moving particles appropriately. Convergence was very slow, and complete equilibrium of the forces was not attained for rigid plates. A large number of plates leads to a tall column, and a small degree of compaction leads to large displacements at the top of the column. Figures 1(a) and 2(a) show the final configurations of stacks of rigid plates. Although the final equilibration of forces does not ensure that plates are at a *stable* equilibrium, in practice no obviously unphysical configurations were observed.

III. FLEXIBLE PLATES

The Laplacian Δ is approximated by the finite difference expression,

$$\Delta\zeta_s^j = a^{-2}(2\zeta_s^j - \zeta_{s-1}^j - \zeta_{s+1}^j) , \tag{5}$$

at interior points $s = 2, \ldots, S-1$, whereas at the ends, the boundary condition (3) implies

$$\Delta\zeta_s^j = 0, \quad s = 1, S .$$

At the $S-2$ interior points of each plate, we have, by (2),

$$\Delta^2\zeta_s^j = a^{-1}f_s^j . \tag{6}$$

For equilibrium, we also require

$$F^j = C^j = 0 , \tag{7}$$

and thus there are S equations for the S unknowns ζ_s^j which define the position of plate j. The equilibrium configuration was determined by an interative scheme. Plates were considered one at a time, and both f_s^j and df_s^j/dx_s^j were computed. The ζ_s^j were then modified so that a solution of the S linear equations (6) and (7) was obtained, using the NAG routine F04ARF [6] (LU factorization with partial pivoting, where L is a lower triangular matrix and U is an upper triangular one). The entire stack of plates was swept, and this procedure was continued until equilibrium was attained.

We nondimensionalize lengths in the x direction by $L = Sa$, and in the z direction by h. Stresses are nondimensionalized by

$$\sigma_0 = Dh/L^4 , \tag{8}$$

where σ_0 is a typical stress required to deflect a plate of aspect ratio L/h through a distance $O(h)$. Nondimensional quantities are denoted by a caret. The governing equations become

$$\frac{d^4\hat{\zeta}^j}{d\hat{x}^4} = \hat{P}, \quad \hat{F}^j = 0, \quad \hat{C}^j = 0 ,$$

and the nondimensional gravitational force per unit area on the plates is

$$\widehat{mg} = G = \frac{mgL^4}{Dh} .$$

The mean vertical compressive stress σ_{zz} in the column of plates varies from 0 at the top surface to N_pSmg/N at the base. The degree of compaction of the stack of plates will depend upon the ratio of the stress to the local effective modulus of the stack. A sufficiently large column of plates would encompass the entire range of behavior, with undeformed plates at the upper surface, and a totally collapsed compact of plates at the base. Simulations of such a tall column would be prohibitively expensive. Instead, a series of simulations were performed, using different values of G. The limit $G = 0$ corresponds to rigid plates. As G increases, the degree of deformation increases, until, for G sufficiently large, even the plates at the top of the stack deform under their own weight. Eventually, the plates become so weak that the spacing of the nodes is determined by the potential (4). This limit was approached, but not quite attained, in the simulations presented here.

In order to determine local effective properties of the stack, the SN_p nodes were first listed in order of increasing z coordinate, and then divided into N_b blocks of B nodes, where $N_bB = SN_p$. The mean number particles in each block is B/S. The dividing surface between blocks may be defined by the surface midway between the topmost nodes of one block and the bottommost nodes of the block immediately above. The top surface of the entire bed is taken to coincide with the upper surface of the plates.

The mean vertical compressive stress in the bottommost block is

$$\sigma_{zz} = (N_b - \tfrac{1}{2})Bmg/N ,$$

and that in the top block is

$$\sigma_{zz} = Bmg/2N ,$$

corresponding to nondimensional stresses $\hat{\sigma}_{zz} = (N_b - \frac{1}{2})BG/N$ and $\hat{\sigma}_{zz} = BG/2N$.

The mean void ratio e within each block is defined as

$$e = \frac{\text{(volume of voids in block)}}{\text{(volume of particles within block)}} .$$

The nodes repel each other *via* soft potentials and therefore never touch. However, it is convenient to consider contact to have occurred if the separation between plate surfaces is less than $\delta = h/100$. One can then define the fraction

$$p_c = \frac{\text{(number of nodes in contact with the node below)}}{\text{(total number of nodes)}} .$$

The bending energy associated with the nodes within the block may be computed by (1). We nondimensionalize energy (per unit length in the y direction) by $E_0 = \sigma_0 hL$, so that

$$\hat{F} = \frac{1}{2S} \sum_{\text{nodes}} \left(\frac{d^2\hat{\zeta}}{d\hat{x}^2} \right)^2$$

and the mean bending energy per plate is

$$\hat{F}_p = \hat{F}S/B \ . \tag{9}$$

IV. RESULTS OF NUMERICAL SIMULATIONS

Figure 1 shows results of a simulation with $N_p = 180, L = 20a$ (i.e., $S = 20$), at a series of increasing values of G. Rigid plates [Fig. 1(a)] act as cantilevers, thereby creating large holes. These rapidly disappear as G increases. The undulating layers of clay are similar to those seen in some shales (Chap. 7 of [1]). In such shales, disruptions to the parallel bedding of clay particles are usually created by the presence of silt particles. In the simulations presented here, the disruptions are created by the edges of the finite clay particles.

Figure 2 shows similar results for a simulation with $L = 10a, N_p = 500$. Note that fluctuations at the top of the stack are large for nonrigid plates. If G is sufficiently large, the vertical position of nodes at any one lattice coordinate x will be independent of the positions of nodes at adjacent lattice coordinates, and we expect fluctuations at the top of the stack to vary as $N_p^{1/2}$. In a real sediment, plates oriented far from the horizontal would slide relative to each other once the yield stress of the compact (or frictional force between plates) was exceeded. There is therefore a need to introduce friction into future simulations, and to allow sliding to occur horizontally as well as vertically.

Figure 3 shows results for the void ratio e as a function of stress σ_{zz}, for three simulations with $(N_p, S) = (500, 5)$, (180,10), and (180,20). Each curve consists of results obtained using many values of G. In order to evaluate average void ratios and stresses within the stacks of plates, the 500 particles of length $S = 5$ were divided into 10 blocks of 250 nodes, whereas the 180 particles of length $S = 10$ and 20 were divided into 9 blocks, of 200 and 400 nodes, respectively. Results for the topmost block were in each case anomalous, and have been discarded. For all three simulations there seems to be a relation of the form

$$e \propto \hat{\sigma}_{zz}^{-0.3}, \quad \hat{\sigma}_{zz} < \sigma_t \ , \tag{10}$$

where the turnover occurs at stresses $\hat{\sigma}_{zz} \simeq \sigma_t = 3 \times 10^4$, 2×10^5, and 10^7 for the cases $S = 5$, 10, and 20, respectively. At higher stresses, the void ratio decreases more rapidly. For $S = 10$ there is a power-law relation of the form

$$e \propto \hat{\sigma}_{zz}^{-1}, \quad \hat{\sigma}_{zz} > \sigma_t \ . \tag{11}$$

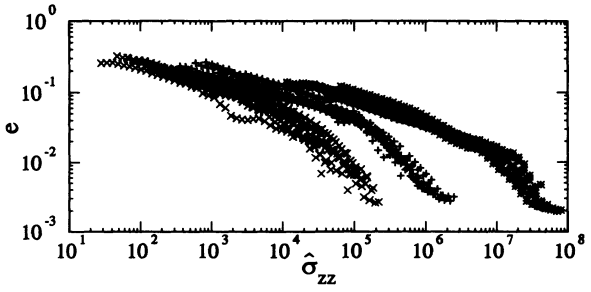

FIG. 3. The void ratio in three compacted beds, as a function of the nondimensional stress $\hat{\sigma}_{zz}$, $\times L = 5a$; $+L = 10a$; $*L = 20a$.

For the other two cases ($S = 5$ and 20) the precise form of the rapid decrease is less clear.

The nondimensionalization adopted in Sec. IV is based on the length of the particles, and one may regard the three sets of results for $S = 5$, 10, and 20 as being obtained on identical particles, using an increasingly fine discretization. One might therefore expect the results to overlap, which they do not. As the mesh size is refined, so the distribution of holes extends to smaller hole sizes, which can withstand higher stresses before collapse. This not only delays the final stages of collapse (i.e., σ_t increases as S becomes large), but also increases the void ratio at any given value of stress $\hat{\sigma}_{zz}$.

At low stresses, the stack of particles is relatively open, with few nodes in contact. As compaction proceeds, additional nodes come into contact, and the packing becomes progressively stiffer. Figure 4 shows the proportion of nodes p_c in contact with the node below. As explained above, this is not well defined: we assume that contact occurs if the node-node separation is less than $\delta = h/100$.

The work W performed in uniaxial compaction from an initial void ratio e_1 and stress σ_1 to a final void ratio e_2 and stress σ_2 takes the form

$$W \propto \int_{e_2}^{e_1} \sigma_{zz} de \ ,$$

and this work is stored within the plates as bending energy F. Hence if

$$e = A\sigma_{zz}^{-\alpha} \ ,$$

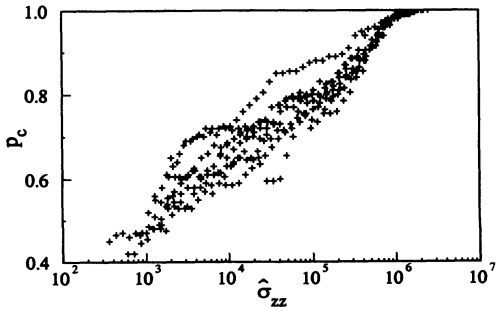

FIG. 4. The fraction p_c of nodes in contact with the node below, as a function of the applied nondimensional stress $\hat{\sigma}_{zz}$. 180 particles of length $L = 10a$.

then the stored energy is

$$F \propto A^{1/\alpha}[e_1^{1-1/\alpha} - e_2^{1-1/\alpha}] = A[\sigma_1^{1-\alpha} - \sigma_2^{1-\alpha}] \ .$$

and we see that we require $\alpha > 1$ if the energy stored in the compact is to remain finite as $e \to 0$. If the plates were described as continuous curves, there would be no limit to the total curvature, and hence to the amount of energy stored within the plates. However, in a discrete simulation, the energy will remain finite. Thus the change behavior from (10) to (11) is again seen to be related to the discreteness of the simulations. At sufficiently high stresses, the soft force (4) between the particles will eventually lead to a void ratio $e \propto \sigma_{zz}^{-1/2}$. We see from Fig. 3 that this limit was not reached in the simulations presented here.

Figure 5 shows the mean bending energy $\hat{F}_p$ stored in the plates, for the case N_p=180, S=10. The bending energy attains a plateau for sufficiently high stresses, and this plateau is higher in blocks further from the horizontal base. At these stress levels, the plates have lost most of their rigidity, and the packing is determined mainly by a local vertical equilibrium. Fluctuations in the height of adjacent nodes forming any given plate are caused by particle edges lower down the stack. A typical fluctuation at height z therefore scales as $(z/S)^{1/2}$. To check this scaling, we computed the sum

$$F_{\rm in} = \frac{a^4}{2h^2}\frac{S}{B(S-2)}\sum(\Delta\zeta_s)^2$$

over each block of B nodes, where $\Delta\zeta_s$ is the finite difference Laplacian (5). The end nodes of each plate do not contribute to $F_{\rm in}$ because of the boundary condition (3), and the factor $S/(S-2)$ makes $F_{\rm in}$ proportional to the average energy per interior node. Once the stack has become compressed, the nth block is bounded between $\hat{z} = (n-1)B/N$ and $\hat{z} = nB/N$, and the mean energy per interior node should scale as $(n-\frac{1}{2})B/NS$. Figure 6 plots

$$F_a = \frac{F_{\rm in}NS}{B(n-\frac{1}{2})} \qquad (12)$$

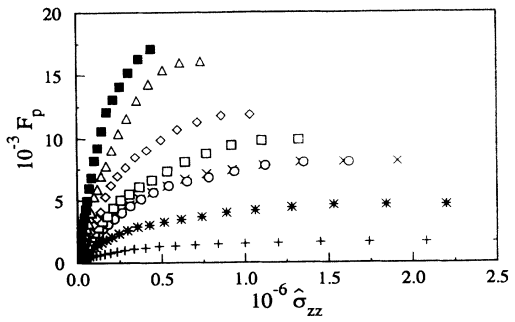

FIG. 5. The nondimensional bending energy per plate F_p as a function of the applied nondimensional stress $\hat{\sigma}_{zz}$. 180 particles of length $L = 10a$. Each curve corresponds to results from one block, with + the block at the base of the stack.

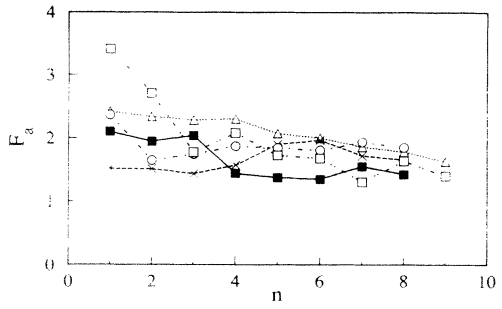

FIG. 6. The scaled energy F_a, defined by (12), plotted against the block number n. Simulations with (N_p, S)=(a) —■— (180,10); (b) ···△··· (500,10); (c) --×-- (180,16); (d) -·-○-·- (180,20); (e) -··-□-·· (500,5).

against the layer number n, for the final compacted state of several simulations. The energy per node scales (roughly) as expected, i.e., F_a varies little between different simulations and between different blocks. Some scatter is to be expected, both because of statistical variations, and because the stresses were insufficiently high for the rigidity of the plates to be completely negligible. We conclude from the results of Fig. 5 that the properties of the stack of plates vary as a function of position z, albeit in a predictable fashion.

V. EXPERIMENTS

In order to test the results of the numerical simulations, we performed an experiment on a quasi-2D packing of flexible platelets. The platelets were pieces of drawing paper of thickness 0.23 mm, with lateral dimensions 25×10 mm^2. Their rigidity modulus, determined by a three-point bending test, was E=0.4 GPa. A container of width 0.3 m and of height 0.5 m was constructed, using two vertical sheets of glass for the front and back. These were held apart by separators of thickness 12 mm, slightly larger than the platelet width in order to avoid excessive friction between the platelets and the container walls. The three separators (forming the base and side walls of the container) were glued onto one of the glass plates, which was held slightly tilted with respect to the vertical. The 5000 paper platelets were then positioned individually, by means of tweezers, with the center of each plate at an abscissa x chosen at random in the range 0–300 mm. If $x < 15$ or $x > 285$, a part of the platelet had to be cut off, in order to avoid overlap with the side walls (separators) at $x = 0$ and 300. When all the platelets were in place, the glass front was clamped onto the cell, which was then held vertically. Compaction of the stack of platelets was performed by dropping a horizontal rod of length 0.26 m into the container, onto the top surface of the stack: the effect of gravity acting on the platelets was negligible compared to the applied stress. The load was the increased by adding further rods, of plastic or metal, to the top of the stack. In spite of some small initial roughness of the stack surface, the loading

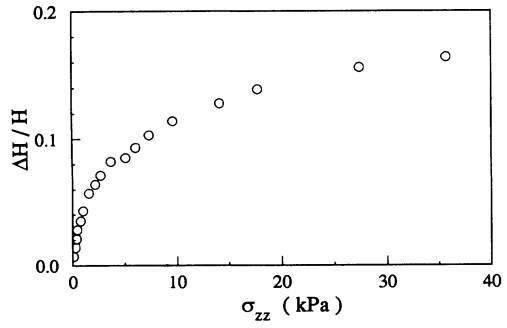

FIG. 7. Experimental results for the stack deformation $\Delta H/H$ as a function of the vertical stress σ_{zz}.

rods were all horizontal. The stress σ_0 defined by (8) is σ_0=0.24 Pa, and the maximum stress 35.7 kPa used in the experiments corresponded to a nondimensional stress $\hat{\sigma}_{zz} = 1.5 \times 10^5$.

The initial height H of the stack was 0.14 m. The maximum loading that we applied induced a deformation $\Delta H/H$=16%. The deformation is shown in Fig. 7 as a function of the applied stress. At each loading a photograph of the stack was taken, showing the progressive deformation of the platelets: four stages of compaction are shown in Fig. 8. Attempts to determine the void ratio e from digitized images proved difficult, and it was easier to compute e by subtracting the volume of the platelets (assumed incompressible) from the total volume of the stack.

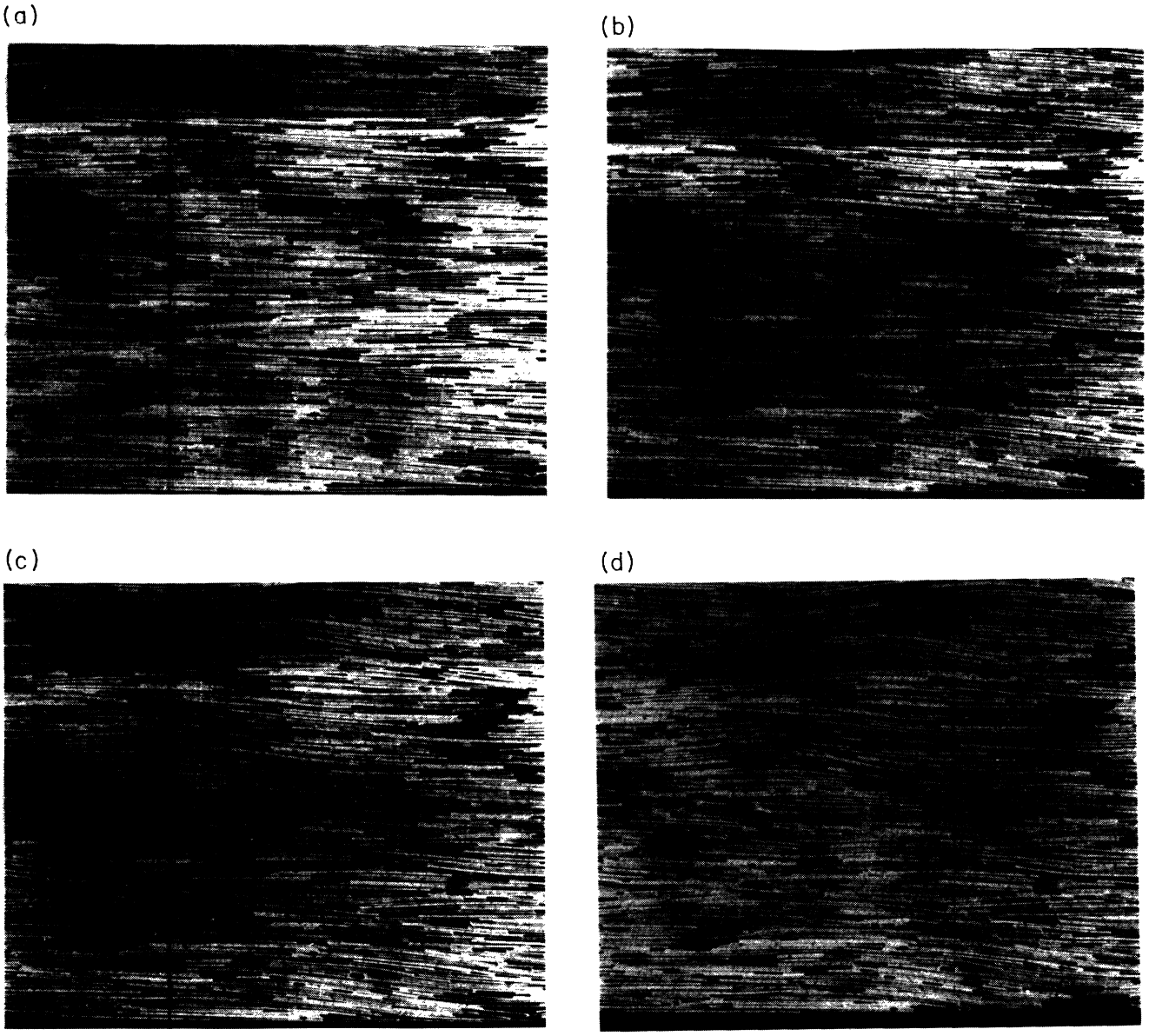

FIG. 8. Bottom part of the stack at four different compactions, $\Delta H/H$= (a) 0; (b) 0.06; (c) 0.11; (d) 0.16.

The results of Fig. 7 indicate $\Delta H/H \propto \sigma_{zz}^{0.7}$ at the lowest stresses, with an exponent which decreases to $\simeq 0.5$ at the highest stresses. Travers *et al.* [7] performed compaction experiments with short cylinders in a quasi-2D cell, similar to our own cell. They obtained a deformation-force relationship of the form $\Delta H/H \propto \sigma_{zz}^{0.26}$, and showed that the nonlinearity was due to an increase in the number of contacts between particles as the load was increased. Presumably, at low stresses, our platelets must deform considerably before each additional contact is formed, and the stress-strain relation is closer to linear than that found for cylinders.

The void ratio is shown in Fig. 9 as a function of the applied stress. Two regimes are observed. At low stresses, the curve does not follow a simple power law: the void ratio tends to a finite limit as the stress decreases to zero. At higher stresses (corresponding to compactions $\Delta H/H > 7\%$), there is a power law, with exponent -0.2. This differs slightly from the exponent -0.3 obtained in the numerical simulations. However, considering the differences between the methods by which stress was applied in the numerical simulation and the experiment, a small difference between the exponents is not surprising.

No attempt has been made here to obtain a distribution of pore (hole) sizes as a function of stress and position in either the numerical simulations or the experiments. This is partly because larger simulations would be desirable for such studies, but also because it is not clear what the most useful measure of pore size would be. A more important goal would be information on the transport properties of the packing, e.g., the permeability to fluid flow. The permeability will be nonzero in a two-dimensional simulation only if the particles are prevented from touching one another, e.g., by electrical repulsions [8]. The extension of the numerical simulations presented here to a three-dimensional packing of flexible plates would at present be prohibitively expensive.

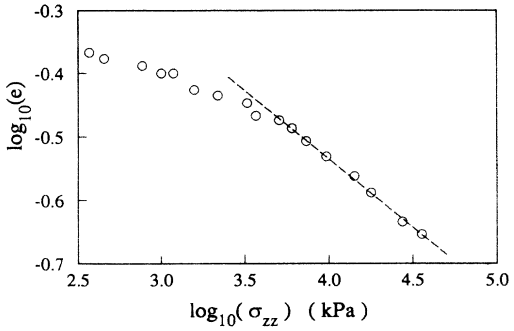

FIG. 9. Experimental results for the void ratio e as a function of the vertical stress σ_{zz}. The broken line corresponds to a power law index -0.216.

[1] N. R. O'Brien and R. M. Slatt, *Argillaceous Rock Atlas* (Springer-Verlag, New York, 1990).
[2] J. D. Sherwood, G. H. Meeten, C. A. Farrow, and N. J. Alderman, J. Chem. Soc. Faraday Trans. **87**, 611 (1991).
[3] H. Van Damme, in *Conferencias Sociedad Espagnola de Arcillas, XI Reunion Cientifica*, edited by E. Gala and M. Ortega Huerta (Universidad de Sevilla, Sevilla, 1992), p. 45.
[4] L. D. Landau and E. M. Lifshitz, *Theory of Elasticity* (Pergamon, Oxford, 1986), Sec. 11.
[5] L. D. Landau and E. M. Lifshitz, *Theory of Elasticity* (Ref. [4]), Sec. 20.
[6] NAG Fortran Library, Mark 15, The Numerical Algorithms Group Ltd., Oxford, UK.
[7] T. Travers, M. Ammi, D. Bideau, A. Gervois, J. C. Messager, and J. P. Troadec, Europhys. Lett. **4**, 329 (1987).
[8] J. D. Sherwood, Proc. R. Soc. London, Ser. A **437**, 607 (1992).

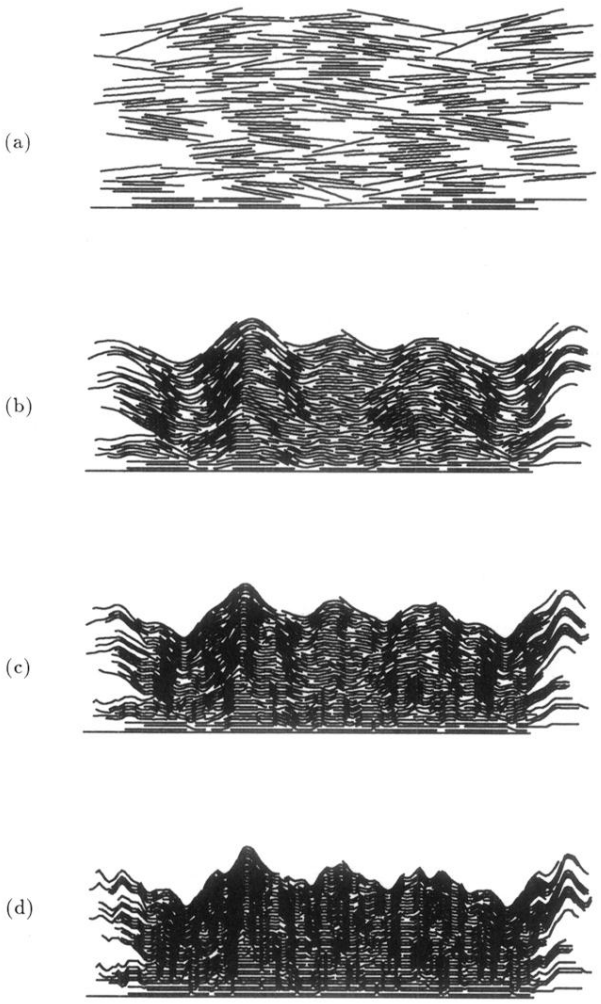

FIG. 1. Simulations of a compacted bed of 180 particles of length $L = 20a$. (a) Rigid plates; (b) $G = 1.9 \times 10^3$; (c) $G = 2.1 \times 10^4$; (d) $G = 1.8 \times 10^5$.

(a)

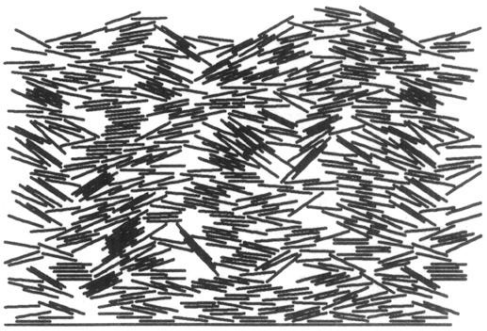

(b)

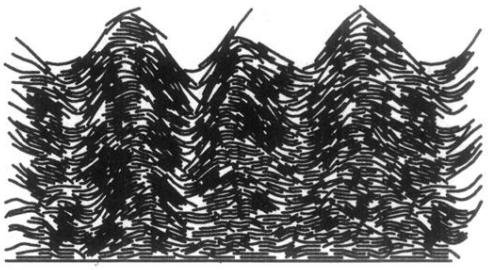

(c)

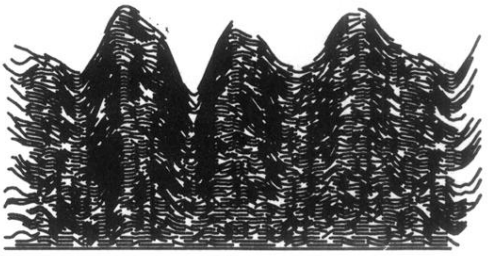

FIG. 2. Simulations of a compacted bed of 500 particles of length $L = 10a$. (a) Rigid plates: (b) $G = 1.2 \times 10^2$; (c) $G = 1.3 \times 10^3$.

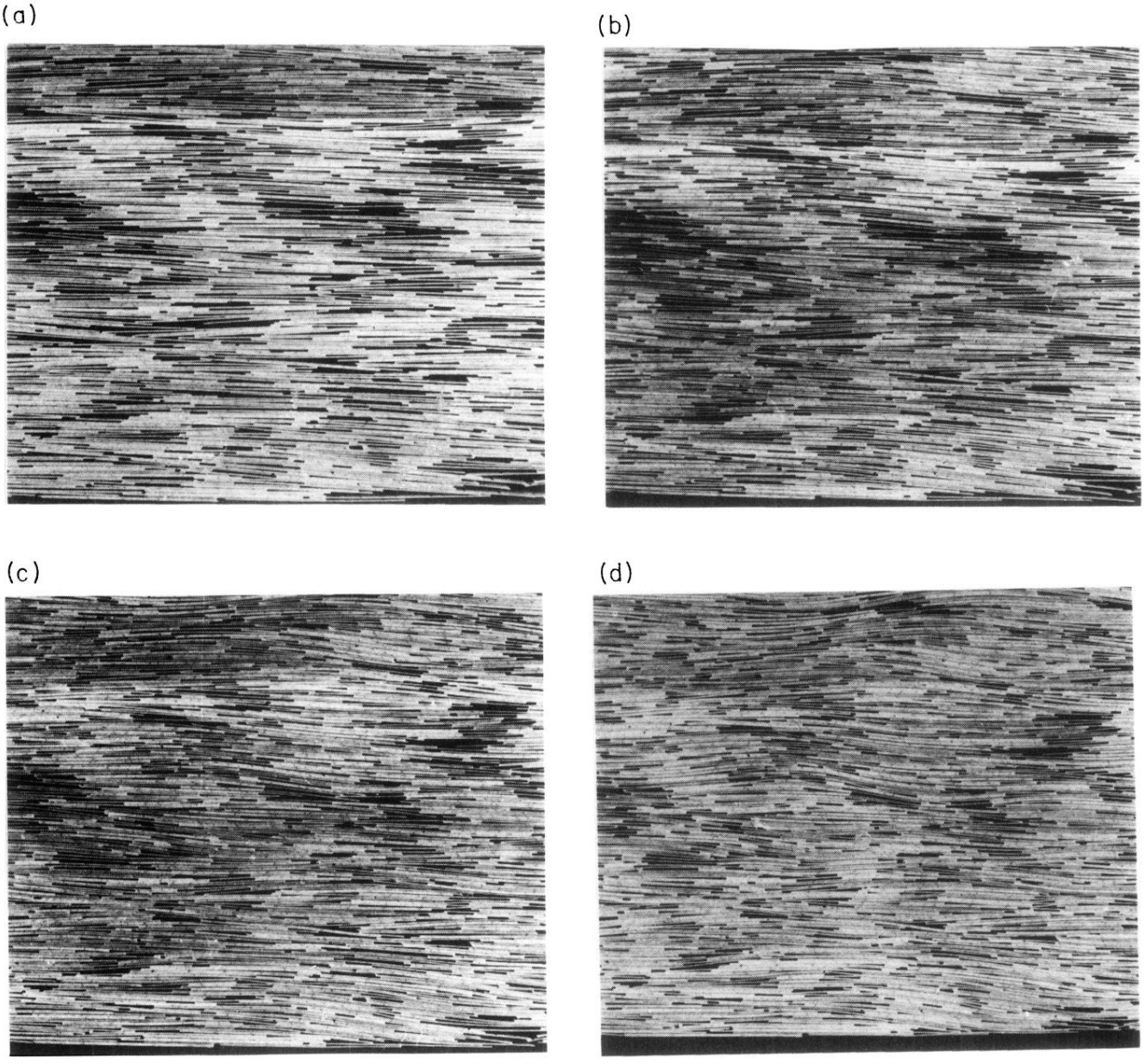

FIG. 8. Bottom part of the stack at four different compactions, $\Delta H/H =$ (a) 0; (b) 0.06; (c) 0.11; (d) 0.16.